Peptides 79 (2016) 103–113

Contents lists available at ScienceDirect

Peptides

journal homepage: www.elsevier.com/locate/peptides

Biochemical and biophysical combined study of bicarinalin, an ant venom antimicrobial peptide

Nathan Téné[a], Elsa Bonnafé[a,1], Fanny Berger[a,1], Aline Rifflet[a], Laure Guilhaudis[b], Isabelle Ségalas-Milazzo[b], Bernard Pipy[c], Agnès Coste[c], Jérôme Leprince[d], Michel Treilhou[a,*]

[a] Equipe EA 4357, VAcBio, Université de Toulouse, CUFR Champollion, Place de Verdun, 81012 Albi, France
[b] Normandie Univ, COBRA, UMR 6014, IRIB, Université de Rouen, INSA de Rouen, CNRS, IRCOF, 1 rue Tesnière, 76821 Mont-Saint-Aignan, France
[c] UMR 152–Pharma-Dev, Université de Toulouse, 31432 Toulouse, France
[d] Inserm U982, Laboratoire de Différenciation et Communication Neuronale et Neuroendocrine, Equipe Facteurs Neurotrophiques et Différenciation Neuronale, Plate-forme de Recherche en Imagerie Cellulaire de Haute-Normandie [PRIMACEN], IRIB, Université de Rouen, 76821 Mont-Saint-Aignan, France

ARTICLE INFO

Article history:
Received 18 February 2016
Received in revised form 31 March 2016
Accepted 1 April 2016
Available online 4 April 2016

Keywords:
Ant venom
Antimicrobial peptide
Therapeutic index [TI]
Prepropeptide
Leishmania
Salmonella
Candida

ABSTRACT

We have recently characterized bicarinalin as the most abundant peptide from the venom of the ant *Tetramorium bicarinatum*. This antimicrobial peptide is active against *Staphylococcus* and Enterobacteriaceae. To further investigate the antimicrobial properties of this cationic and cysteine-free peptide, we have studied its antibacterial, antifungal and antiparasitic activities on a large array of microorganisms. Bicarinalin was active against fifteen microorganisms with minimal inhibitory concentrations ranging from 2 and 25 μmol L^{-1}. *Cronobacter sakazakii*, *Salmonella enterica*, *Candida albicans*, *Aspergilus niger* and *Saccharomyces cerevisiae* were particularly susceptible to this novel antimicrobial peptide. Resistant strains of *Staphylococcus aureus*, *Pseudomonas aeruginosa* and *C. albicans* were as susceptible as the canonical strains. Interestingly, bicarinalin was also active against the parasite *Leishmania infantum* with a minimal inhibitory concentrations of 2 μmol L^{-1}. The bicarinalin pre-propeptide cDNA sequence has been determined using a combination of degenerated primers with RACE PCR strategy. Interestingly, the N-terminal domain of bicarinalin pre-propeptide exhibited sequence similarity with the pilosulin antimicrobial peptide family previously described in the *Myrmecia* venoms. Moreover, using SYTOX green uptake assay, we showed that, for all the tested microorganisms, bicarinalin acted through a membrane permeabilization mechanism. Two dimensional-NMR experiments showed that bicarinalin displayed a 10 residue-long α-helical structure flanked by two N- and C-terminal disordered regions. This partially amphipathic helix may explain the membrane permeabilization mechanism of bicarinalin observed in this study. Finally, therapeutic value of bicarinalin was highlighted by its low cytotoxicity against human lymphocytes at bactericidal concentrations and its long half-life in human serum which was around 15 h.

1. Introduction

Classical antibiotics are under intense pressure from emerging resistance and antimicrobial peptides (AMPs) are now considered as credible alternatives in the development of novel biocidal agents [1,2]. AMPs play important roles in preventing infections by providing an effective and fast acting defense against harmful microorganisms [3–5]. Furthermore, they display an ability to efficiently destroy a broad spectrum of microorganisms and particularly, multi-drug-resistant (MDR) bacteria. AMPs are generally small amphipathic cationic peptides of variable length (12–30 amino acids), active against bacteria, parasites, yeasts, fungi, viruses and tumour cells [6–8]. They usually act through relatively non-specific processes resulting in a membranolytic activity based on pore formations by barrel-stave, carpet or toroidal-pore mechanisms [3,9,10]. Physical interactions between AMP and microorganisms such as charge–charge and hydrophobic contacts might explain why development of resistance against cationic peptides is difficult. When these natural AMPs exhibit substantial cytotoxicity towards eukaryotic cells, a decrease in their hydrophobicity, helicity and amphipathicity, by replacing specific

* Corresponding author.
E-mail address: michel.treilhou@univ-jfc.fr (M. Treilhou).
[1] These authors contributed equally to this study.

http://dx.doi.org/10.1016/j.peptides.2016.04.001
0196-9781/

amino-acids by cationic residues, reduces hemolytic activity and concomitantly promotes antibacterial potency, turning them into therapeutically valuable anti-infective agents [11].

Venoms of arthropods are a rich source of biologically active compounds [12–15]. With 13,161 known species, ants constitute a highly diversified group of arthropods [16]. AMPs have been identified in several species, such as pilosulins from the Australian *Myrmecia pilosula* [17,18] or ponericins from the neotropical ant *Pachycondyla goeldii* [19]. Unlike stingless species which typically spray or deposit small molecules such as formic acid, most stinging ants have evolved complex venoms particularly rich in peptides and enzymes [20]. This is the case for the *Tetramorium* genus for which the venoms are predominantly proteinaceous [21]. The discovery of novel AMPs is scientifically challenging and their development as drugs is often limited due to the lack of detailed data on their physicochemical characteristics [2,5]. Especially, pharmacological and pharmacokinetic data describing their mechanism of action and their physicochemical properties, respectively, are generally missing.

Bicarinalin is a cystein-free polycationic linear and amidated peptide, active against Staphylococcus and Enterobacteriaceae strains. It exhibits a very low hemolytic activity against human red blood cells [21].

The first aim of the present study was to further investigate the biological activities of bicarinalin against a large collection of microorganisms such as bacteria, fungi, yeasts and a parasite, to determine its cytotoxicity on human lymphocytes and its stability in human serum. Then, in order to gain further insight into the structure of ant toxin precursors, we also investigated the pre-probicarinalin cDNA organisation using a RACE PCR strategy. Finally, we explored its mechanism of action and determined its solution structure using two dimensional (2D) ^{1}H NMR and molecular dynamics.

2. Materials and methods

2.1. Peptide synthesis

Bicarinalin (KIKIPWGKVKDFLVGGMKAV-NH_2), its randomly-designed amidated scrambled counterpart (VVMKLGKAFVPIGKWKKDGI-NH_2) and bicarinalin$_{(4–20)}$ (IPWGKVKDFLVGGMKAV-NH_2) were synthesized on a Liberty microwave assisted automated peptide synthesizer (CEM, Saclay, France) at a purity grade higher than 99% as previously described [21]. The scrambled counterpart was randomly designed from bicarinalin amino-acids ensuring a total disrupting of the native helix as predicted by Agadir program and was used as negative control. The authenticity and the molecular identity of the synthetic peptides were controlled by MALDI-TOF-MS.

2.1.1. Reagents and microorganisms

All chemical reagents (melittin, ampicillin, tetracycline, SYTOX green, fluconazole and methicillin) were obtained from Sigma-Aldrich (Saint-Quentin-Falavier, France). Trifluoroethanol-d_2 (TFE-d_2) was from SDS (Peypin, France). Referenced bacterial strains were purchased from Institut Pasteur (CIP) and/or AES Biomerieux (ATCC). All microorganisms were grown in broth medium with continuous shaking at 150 rpm. The Gram negative strains used were *Pseudomonas aeruginosa* (CIP 82118 and multiresistant ATCC 15442), *Cronobacter sakazakii* (ATCC 29544), *Escherichia coli* (CIP 7624) and *Salmonella enterica* (ATCC 29934). *Enterococcus hirae* (CIP 5855), *Bacillus subtilis* (CIP 5262), *Staphylococcus aureus* (CIP 53156) and MRSA resistant to methicillin and oxacillin (ATCC 43300), and *Staphylococcus xylosus* (ATCC 35033) were used as Gram positive strains. Fungal and yeast strains used were *Geotrichum candidum* (ATCC 204307), *Aspergillus niger* (CIP 143183), *Saccharomyces cerevisiae sp*. and *Candida albicans* (CIP 4872 and wild multiresistant (CAAL 117; Supplementary Table 1). Bacteria were grown in tryptic soy broth at 37 °C (except for *S. aureus* and *C. sakazakii*, 40 °C) while fungi and yeast were grown in Sabouraud broth at 30 °C. After incubation, 100 μL of bacteria inoculum were suspended in 5 mL fresh broth medium for 4 h to obtain a mid-log-phase culture which was diluted in the same medium, to an absorbance of 0.002 at λ_{max} = 600 nm.

2.1.2. Antimicrobial activity

Minimal inhibitory concentrations (MIC) of native and scrambled bicarinalin were determined by a standard two-fold dilution method as previously described [22]. Bacteria were incubated with different concentrations of each compound (from 0.05 to 97.5 μmol L^{-1} for bicarinalin and melittin, and from 0.049 to 100 μmol L^{-1} for other antibiotics) in 100 μL final volume of soy broth medium (10^4 to 10^5 CFU). The microplates were incubated 24 h at specific temperature with continuous shaking. Absorbance was measured at the wavelength of 600 nm using a spectrophotometric microplate reader (Infinite 200, Tecan, Lyon, France). MICs were expressed as the lowest concentration demonstrating no visible growth. Phosphate buffered saline (PBS) and scrambled bicarinalin were used as a negative control while conventional antibiotics were used as positive controls. The minimal bactericidal concentration (MBC) value was established by counting the colony growth on an inoculated agar plate after 24 h of incubation with different concentrations (≥MIC) as previously described [22]. They were expressed as the lowest concentration that caused a 99.9% reduction of the initial inoculum.

2.1.3. Antiparasitic activity

The proliferation of axenic *Leishmania infantum* (MHOM/MA/67/ITMAP-263) amastigotes expressing luciferase activity was evaluated in Rosswell Park Memorial Institute medium containing 10% fetal calf serum for 48 h at 25 °C in presence of native or scrambled bicarinalin. Their leishmanicidal activity was measured for concentrations ranging from 0.05 to 97.5 μmol L^{-1}. The luciferase substrate (Promega, Lyon, France) was added after incubation and its activity was measured using a luminometer following the conditions described by Sereno et al. [23].

2.1.4. Membrane permeabilization assay

The membrane permeabilization of each strain by bicarinalin was evaluated using SYTOX green uptake assay as previously described [20]. Briefly, SYTOX green was added to these bacteria suspensions (optical density adjusted to 0.6 at the wavelength of 600 nm) at a final concentration of 0.5 μmol L^{-1}. After distribution into a micro-well plate with 100 μL of each bacterial suspension, bicarinalin was added to perform a serial two-fold dilution (same range of concentrations as above). After 30 min of incubation, SYTOX green uptake was recorded by using an Infinite 200 spectrophotometric microplate reader (λ_{ex} 488 nm, λ_{em} 540 nm).

Lymphocyte isolation and cell cytotoxicity assay

Lymphocytes were isolated from total heparinized blood samples obtained from one healthy donor using Ficoll-PlaqueTM PLUS kit (GE healthcare, Toulouse, France). After two washes in PBS, lymphocytes were suspended in PB-MaxTM medium supplemented with 1% of bovine serum albumin, 100 μg.mL^{-1} of streptomycine, 100 U/mL of penicillin and 2 mmol L^{-1} of glutamine. Viability and numbering of the cells were determined using trypan blue stain 0.4% and Malassez hemocytometer.

The lactate deshydrogenase (LDH) cytotoxicity assay kit (Life Technologies) was used to determine the cytotoxic effect of bicarinalin. Lymphocytes were incubated in triplicate into a 96-well plate overnight with various concentrations of bicarinalin in PB-MaxTM

medium at 37 °C in a 5% CO_2 atmosphere. Supernatants were then analyzed for LDH activity detection by measuring the absorbance at 490 nm following manufacturer's instructions. Controls of maximum and spontaneous LDH activity were also done in triplicate to calculate the percentage of cytotoxicity.

2.1.5. Serum stability

Bicarinalin was incubated with 90% fresh normal human serum at 37 °C until 48 h. Antimicrobial activity against *S. aureus* was evaluated as described above. For LC–MS analysis, incubation was stopped by adding trifluoroacetic acid (10% of the final volume) and the samples were diluted in water.

2.1.6. Total RNA extraction and full length bicarinalin cDNA cloning

Ants were frozen and venom glands were dissected on ice under stereomicroscope. Total RNA was then extracted using TRIzol reagent (Invitrogen, Waltham, MA) according to the manufacturer's protocols. Contaminating genomic DNA was removed using DNA-free Kit (Applied Biosystem, Waltham, MA). RNA quantity was evaluated using a Nanodrop 2000. For 3′cDNA cloning, a RT was performed using 500 ng of total RNA with M-MLV and 3′RACE adapter from the FirstChoice RLM-RACE Kit (Invitrogen). A 3′RACE PCR was performed with an outer degenerated primer (OuterPe, "AARATHAARATHCCNTGGGG") and the Outer 3′RACE primer from FirstChoice RLM-RACE Kit followed by a second PCR using an inner degenerated primer (InnerPe, "AARGTNAARGAYTTYYTGG") and the Inner 3′RACE primer from the FirstChoice® RLM-RACE to increase PCR product specificity. Degenerated primers were designed based on the N-terminal end of the peptide. The approximately 300 bp PCR product was cloned into pCR®II vector using TA-cloning Kit Dual promoter pCR®II (Invitrogen) and sequenced with M13 reverse and forward (-20) primers (Get-TQ, Toulouse, France).

5′RACE specific primers were then designed with the 3′cDNA sequence (5RACEoutPe "CAATCTTCCTCGTAGGTTGC" and 5RACEInPe "ACTTCTTTCCCACGGCTTTC") using eprimer3 (http://mobyle.pasteur.fr/). 5′cDNA end was obtained using FirstChoice RLM-RACE Kit according to the manufacturer's instructions. PCR product was cloned and sequenced using the same protocol described for 3′cDNA end.

2.1.7. Sequence analysis

Sequences were analyzed using Mobyle@Pasteur portal (http://mobyle.pasteur.fr/). The amino acid sequence was deduced using EMBOSS 6.3.1 transeq program. The homology searches of nucleotide and protein sequence were conducted with BLAST program on NCBI and Uniprot (http://www.ncbi.nlm.nih.gov/, www.uniprot.org/). The amino acid sequence was then analyzed to search predicted signal sequence, cleavage sites and secondary structures with EMBOSS 6.3.1 Patmatmotifs, Sigcleave and Garnier softwares, respectively. Phylogenetic analyses were conducted using Quicktree 1.1 software with the neighbor joining method.

2.1.8. Nuclear magnetic resonance (NMR) analysis

NMR experiments were performed on a Bruker Avance III 600 MHz spectrometer (Wissembourg, France), equipped with a triple resonance cryoprobe including shielded z-gradients. Bicarinalin was dissolved in a water/TFE-d_2 mixture (1:1, v/v) at a concentration of 1 mmol L^{-1}. Two dimensional COSY, TOCSY and NOESY experiments were carried out at 298 K. TOCSY was performed with a 80 ms DIPSI mixing. NOESY spectra were collected at mixing times of 120, 150 and 200 ms. Experiments were acquired with excitation sculpting water suppression except for COSY where a low power pre-saturation was used. TOCSY and NOESY experiments were performed in the phase-sensitive mode, using States-TPPI method. Proton chemical shifts were reported related to TFE as an internal reference. Distance restraints for NOE diagram and structure calculations were derived from cross-peaks in the 150 ms NOESY. NOE cross-peaks were converted into distances by volume integration using Felix NMR software (FELIX Corporate Headquarters, San Diego, CA). The NOE volumes between Pro^5 geminal H_δ and Asp^{11} geminal Hβ protons, which correspond to a distance of 1.8 Å were used for calibration. The consistency of this calibration was verified on the other geminal proton distances. A range of ±25% of the calculated distance was used to define the upper and lower bounds of the restraints between H_N, Hα, and Hβ atoms. For the other restraints, a range of ±12.5% of the squared calculated distance was used to take into account spin diffusion.

2.1.9. 3D structure calculations

Three-dimensional structures were calculated *in vacuo* with the program CNS [24] and the force field CHARMM22. A protocol adapted from Stein et al. [25], consisting of four molecular dynamics simulated annealing and minimization stages, both in torsion angle and Cartesian spaces, was used: (*i*) a high-temperature torsion angle dynamics phase at 20,000 K (15 ps, NOE energy weight = 150) using an extended conformation; (*ii*) a torsion angle dynamics slow-cooling phase from 20,000 to 0 K (30 ps, temperature cooling step = 250 K, w_{NOE} = 150). This first slow-cooling phase allowed to increase the scale factor of van der Waals energy term from 0.1 to 1; (*iii*) a Cartesian dynamics cooling phase from 2000 to 0 K (15 ps, temperature cooling step = 250 K, w_{NOE} = 150). This second slow-cooling phase allowed to increase the scale factor of van der Waals energy term from 1 to 4 and (*iv*) a final Powell minimization (20,000 steps; gradient tolerance = 0.05, w_{NOE} = 50).

A total of 130 unambiguous and 26 ambiguous distance restraints were used for the calculations. A set of 100 structures was generated and the 64 conformers presenting no systematic distance violation larger than 0.2 Å were selected as final structures. These final structures were analyzed using CNS and homemade scripts and displayed with SYBYL package (Tripos Associates, St. Louis, MO) and MOLSCRIPT [26].

2.1.10. Data and statistical analysis

MIC, MBC and fluorescence measurements were performed in triplicate. Curves were built by plotting the averages of absorbance or fluorescence values ± SEM as a function of the concentration of peptide or antibiotic and analyzed with GraphPrism 5 software. The LC_{50} values were obtained from concentration–response curve using a sigmoidal dose-response fit with variable slope.

3. Results

3.1. Antimicrobial activities

Bicarinalin was active against the fifteen strains tested including bacteria and fungi, with MICs values ranging from 0.45 (*S. xylosus*) to 97.5 μmol L^{-1} (*G. candidum*) (Table 1). It was particularly potent on Gram-negative bacteria even against MDR strains. Indeed, MICs were as low as referenced antibiotics. For the multi-resistant *P. aeruginosa* strain, the MIC was lower than 12.2 μmol L^{-1} (standard strain), while melittin and standard antibiotics were weakly active. With a MIC of 5.4 μmol L^{-1}, *S. enterica* was the most susceptible Gram-negative bacteria. Except for *B. subtilis*, bicarinalin was also particularly effective against Gram-positive bacteria with MICs equal to or lower than 12.2 μmol L^{-1}. It was less potent than ampicillin and tetracycline against *E. hirae* and standard strain of *S. aureus* and than melittin, tetracycline and methicillin against *MRSA*.

Regarding fungi and yeasts, bicarinalin was less active against *G. candidum* but more active against *A. niger*, *S. cerevisiae* and

Table 1
In vitro antimicrobial activities of bicarinalin against bacteria, fungi and a parasite.

Microorganisms	MIC[c, e] [μmol L^{-1}]						MBC[d,e] [μmol L^{-1}]
	Bicarinalin	Melittin	Ampicillin	Tetracycline	Methicillin	Fluconazole	Bicarinalin
Gram-Negative Bacteria							
E. coli [a]CIP 7624	24.4	22.4	25.0	33.7	nt	nt	24.4
C. sakazakii [b]ATCC 29544	5.80	17.20	12.52	44.0	nt	nt	6.1
P. aeruginosa CIP 82118	12.2	73.9	19.0	69.6	nt	nt	24.4
P. aeruginosa [R]ATCC 15442	8.7	74.5	> 100	69.0	nt	nt	12.2
S. enterica ATCC 29934	5.4	52.7	3.1	8.4	nt	nt	6.1
Gram-Positive Bacteria							
E. hirae CIP 5855	12.2	> 97.5	0.2	4.2	nt	nt	12.2
S. aureus CIP 53156	3.0	3.5	0.4	1.0	2.4	nt	3.0
MRSA ATCC 43300	8.7	3.4	> 100	1.2	4.9	nt	12.2
S. xylosus ATCC 35033	0.45	2.6	0.81	13.0	nt	nt	0.76
B. substilis CIP 5262	24.4	89.6	12.0	36.0	nt	nt	24.4
Fungi							
A. niger CIP 143183	0.75	0.69	nt	nt	nt	6.5[f]	0.76
C. albicans CIP 4872	17.3	4.6	nt	nt	nt	0.8[f]	24.4
C. albicans [R],[g] CAAL 117	17.3	3.3	nt	nt	nt	209[g]	24.4
G. candidum ATCC 204307	97.5	89.6	nt	nt	nt	13.1	97.5
S. cerevisiae sp	6.1	44.8	nt	nt	nt	26.1	6.1
Parasite							
L. infantum	1.5	nt	nt	nt	nt	nt	–

[R]: multi-resistant strains.
Nt: non tested.
[a] CIP, Collection de l'Institut Pasteur, Paris, France.
[b] ATCC, American Type Culture Collection, Manassas, VA.
[c] MIC: Minimal inhibitory concentration.
[d] MBC: Minimal bactericidal concentration.
[e] Mean values of three independent experiments performed in duplicate.
[f] Data from Nemati et al., 2013 [27].
[g] Strain and data from the Nantes Hospital [France].

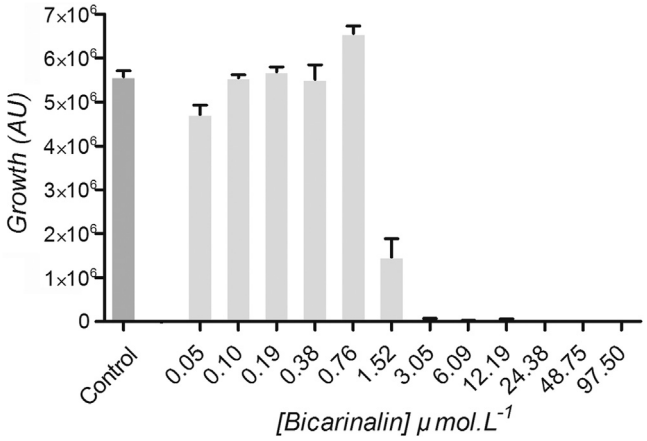

Fig. 1. Growth of *L. infantum* in presence of increasing concentrations of bicarinalin. Data are mean ± SEM of independent experiments performed in triplicate.

resistant *C. albicans* than fluconazole. No activities were detected for scrambled bicarinalin under 97.5 μmol L^{-1}.

The MBCs values (Table 1) were consistent with the corresponding MICs, except for *P. aeruginosa, MRSA, S. xylosus* and *C. albicans* strains for which the MBCs were about 1.4–2 folds the corresponding MICs. For each strain, the low ratio MBC/MIC confirmed the bactericidal property of bicarinalin.

3.2. Antiparasitic activity

As shown in Fig. 1, bicarinalin had a high antiparasitic activity against *Leishmania infantum*. The peptide dose-dependently inhibited the growth of this parasite from 1.5 μmol L^{-1}, which corresponded to the MIC (Table 1). Scrambled counterpart was not active against *L. infantum*.

3.3. Plasma membrane permeabilization

In order to correlate the antimicrobial activity of bicarinalin to a putative membranolytic action, its effect on the membranes of living bacteria has been investigated using the fluorescence of SYTOX green, a membrane non permeant DNA-binding dye. For all microorganisms, fluorescence increased exactly when bacterial/fungal growth decreased, showing a correlation between microorganism death and membrane permeabilization (Fig. 2, for *P. aeruginosa*, *E. hirae* and *C. albicans*). For all bacteria, we obtained the same profiles (growth/fluorescence) than for our previous data against Enterobacteriaceae [22].

3.4. Cytotoxicity

Bicarinalin displayed no cytotoxicity against human lymphocytes in concentrations ranging from 0.066 to 8.5 μmol L^{-1} and its LC_{50} value was 67.8 μmol L^{-1} (Fig. 3), i.e. around 10-fold above the median of the measured MICs.

3.5. Susceptibility of bicarinalin to enzymatic degradation in human serum

Bicarinalin retained its efficiency against *S. aureus* after 10 h of incubation in serum. Its biological half-life was around 15 h. After 20 h, the antimicrobial activity was lost (Fig. 4a). In order to correlate this loss of activity with the degradation, we analyzed the corresponding incubation medium by LC–MS. During the first three hours we observed only the [m/z = 1107.45] corresponding to the $[M+2H]^{2+}$ of native bicarinalin. Between the third and the tenth hour, bicarinalin signal decreased (Fig. 4b) and degrada-

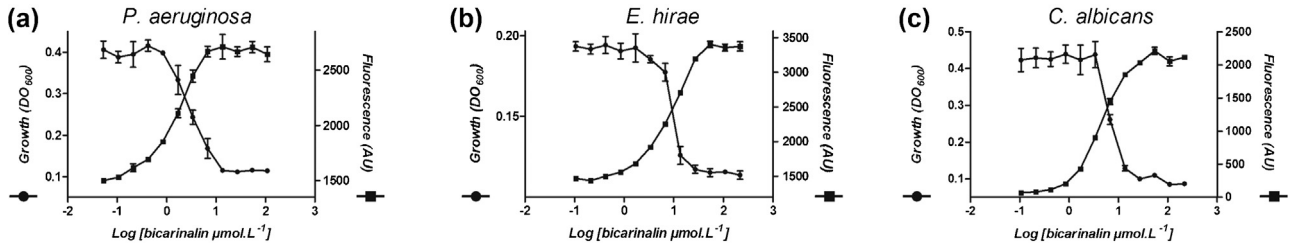

Fig. 2. Dose-response curves of membrane permeabilization induced by bicarinalin on selected bacteria: **[a]** *P. aeruginosa*, **[b]** *E. hirae*, **[c]** *C. albicans*. For each strain, growth [left y axis ●] and fluorescence [right y axis ■] variations are shown in terms of the logarithm of bicarinalin concentration. Membrane permeabilization was measured in triplicate using the SYTOX green DNA-binding dye as described above and expressed as mean ± SEM. The net uptake of the dye through the plasma membrane was monitored by fluorescence at 540 nm.

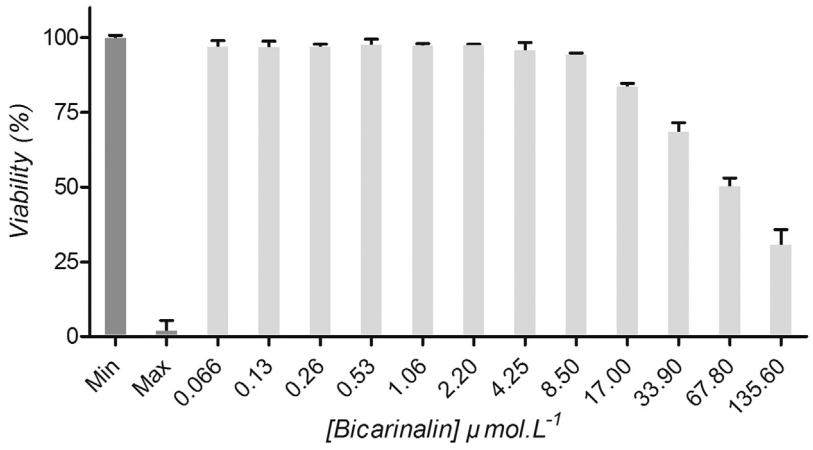

Fig. 3. Effect of increasing concentrations of bicarinalin on human lymphocyte survival. Data are mean ± SEM of independent experiments performed in triplicate.

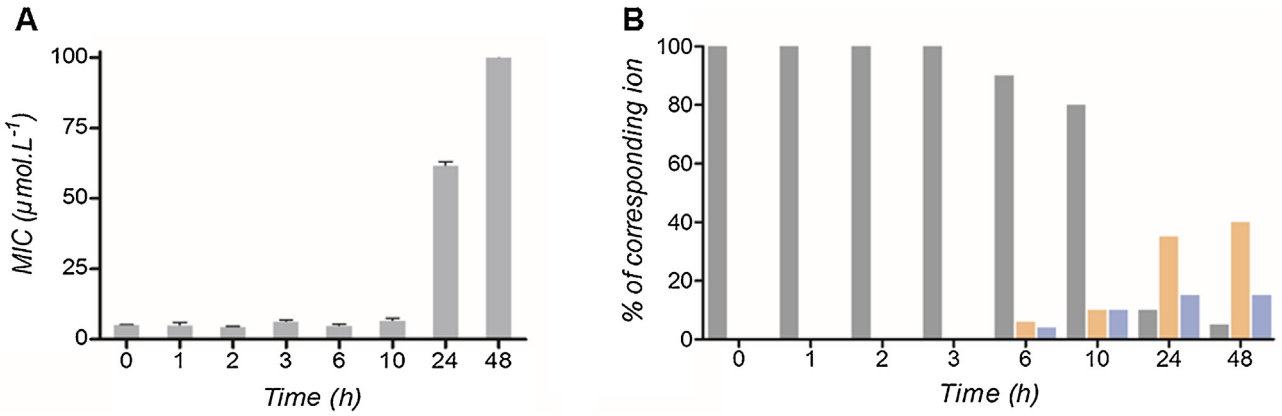

Fig. 4. [a] Time-course of bicarinalin activity in human serum [37 °C]. Estimated biological half-life around 15 h **[b]** Monitoring of bicarinalin degradation: bicarinalin [m/z = 1107.45 $[M+2H]^{+2}$, grey bars] and metabolites formation [desLys[1]] bicarinalin [m/z = 1043.12 $[M+2H]^{+2}$, orange bars] and bicarinalin [4–20] [m/z = 922.53 $[M+2H]^{+2}$, blue bars] in serum by liquid chromatography coupled to mass spectrometry. (For interpretation of the references to colour in this figure legend, the reader is referred to the web version of this article.)

tion products appeared, with ions $[M+2H]^{2+}$ at m/z 1043.12 and 922.53 consistent with the loss of the N-terminal lysine and the first three N-terminal residues (KIK, bicarinalin$_{(4-20)}$), respectively. After 24 h of incubation, bicarinalin$_{(4-20)}$ was the main degradation product remaining although in a weak abundance. No other degradation product was detected. Synthetic bicarinalin$_{(4-20)}$ has been tested for its antimicrobial activity and showed a MIC of 9 μmol L^{-1} against *S. aureus*, in comparison to 3 μmol L^{-1} for bicarinalin (Supplementary Table 2).

3.6. Characterization of T. bicarinatum pre-probicarinalin cDNA

Amino acid sequences of AMPs are divergent, conversely to the propeptide sequences (N-terminal) that are mostly conserved and used to classify these peptides into families [28]. Since bicarinalin exhibits no meaningful sequence similarity with any known peptides, we have cloned its complete precursor cDNA (accession number KF929552) to establish to which family bicarinalin belonged and to predict its processing. Using degenerated primers combined with RACE PCR strategies, we have cloned a 525 pb full length cDNA that encoded a predicted ORF of 89 amino acids. Analysis of cDNA sequence revealed a destabilizing AUUUA motif

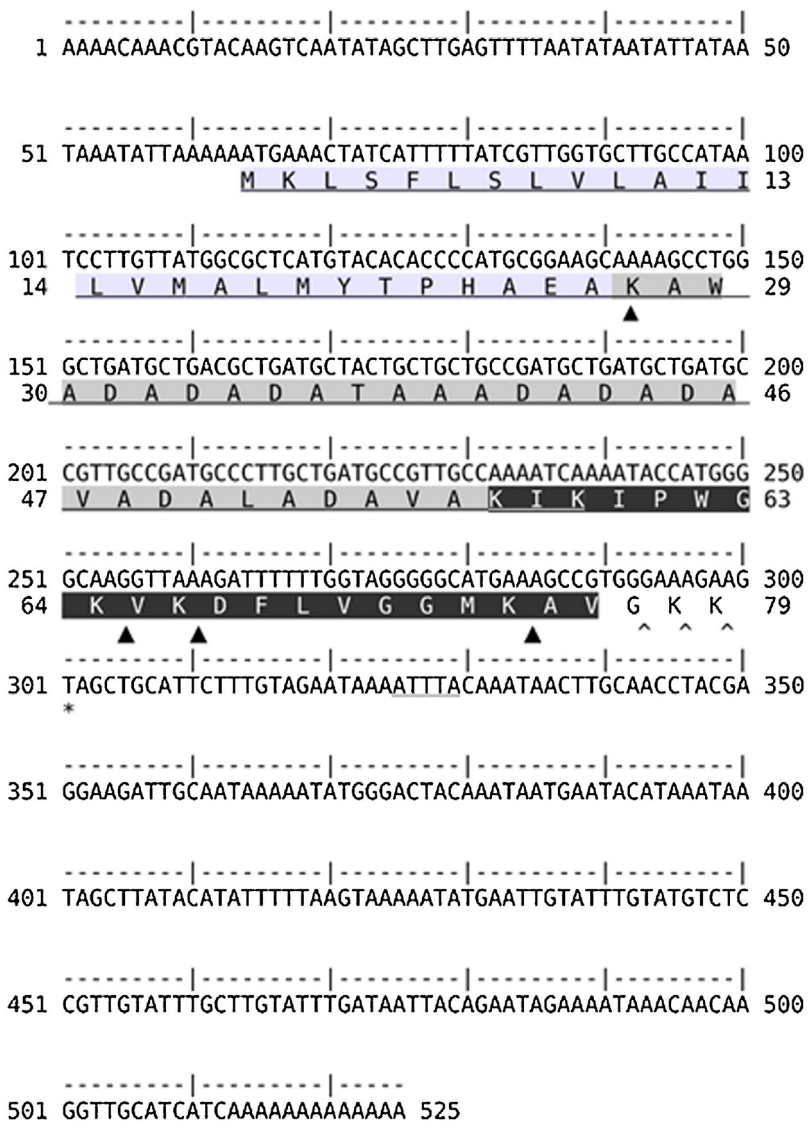

Fig. 5. Full length cDNA of bicarinalin and predicted amino acid sequence [accession number KF929552]. The mature peptide sequence is highlighted in black. The underlined region is a predictive alpha helix. In light grey: putative hydrophobic signal peptide. In grey: putative propeptide sequence. ˆindicates the amidation signal. ▲ indicates potential cleavage sites. Garnier and Predator softwares didn't predict an alpha helix in the mature peptide.

(Fig. 5) in the 3′UTR. Bicarinalin precursor showed a classical organisation with a signal peptide of 26 residues, as predicted by the Sigcleave program, a downstream propeptide of 30 amino acids followed, without conventional processing site, by the bicarinalin sequence located in the C-terminal region of the precursor. Bicarinalin sequence was followed by a conventional C-terminal Gly-Lys-Lys amidation signal [29]. Blast analysis on Uniprot and Genbank revealed similarity of the N-terminal part [residue 1–56] with pre-propilosulin-1, −3, −4 and −5 (56% of similarity with pilosulin-5 of *Myrmecia banksi*, Evalue = 10^{-11}). Alignment with pilosulin pre-propeptide sequences revealed a strong conservation in the cleavage sites of signal peptide of the pre-propeptides (consensus motif EAK) (Fig. 6a). However, there was no conservation in the cleavage sites of propeptides. Mature sequence peptides shared poor similarity except for the presence of lysine at four conserved positions that conferred a cationic property to these peptides. Phylogenetic analysis using Quicktree 1.1 program (Fig. 6b) revealed that bicarinalin was located in a branch with pilosulin-5.

3.7. Identification of secondary structural elements by NMR

The bicarinalin conformation was investigated by NMR in a TFE/water (1:1 v/v) mixture, a medium known for stabilizing linear short peptide secondary structures. The proton resonance assignment was carried out using a classical strategy [30]. Spin systems were identified using a combination of 2D TOCSY and COSY spectra and neighboring residues were connected through 2D NOESY experiments. A first assessment of bicarinalin secondary structure was obtained by analyzing Hα chemical shifts, as their deviations from the random coil values are representative of peptide secondary structure. A 2D NOESY spectrum with a mixing time of 150 ms was also recorded to improve this estimate with a detailed analysis of sequential and medium range inter residue NOEs. The Hα secondary chemical deviations (CSD) calculated for bicarinalin strongly suggested the presence of a helical conformation between residues Val^9 and Lys^{18} (Fig. 7a). This helical conformation could be extended in the N-terminal region to residues Trp^6, Gly^7 and Lys^8. Surprisingly, for this lysine residue, the Hα CSD was null. Nevertheless, the low CSD values observed for Trp^6 and Gly^7 Hα suggested the presence of a helical structuration between Trp^6 and

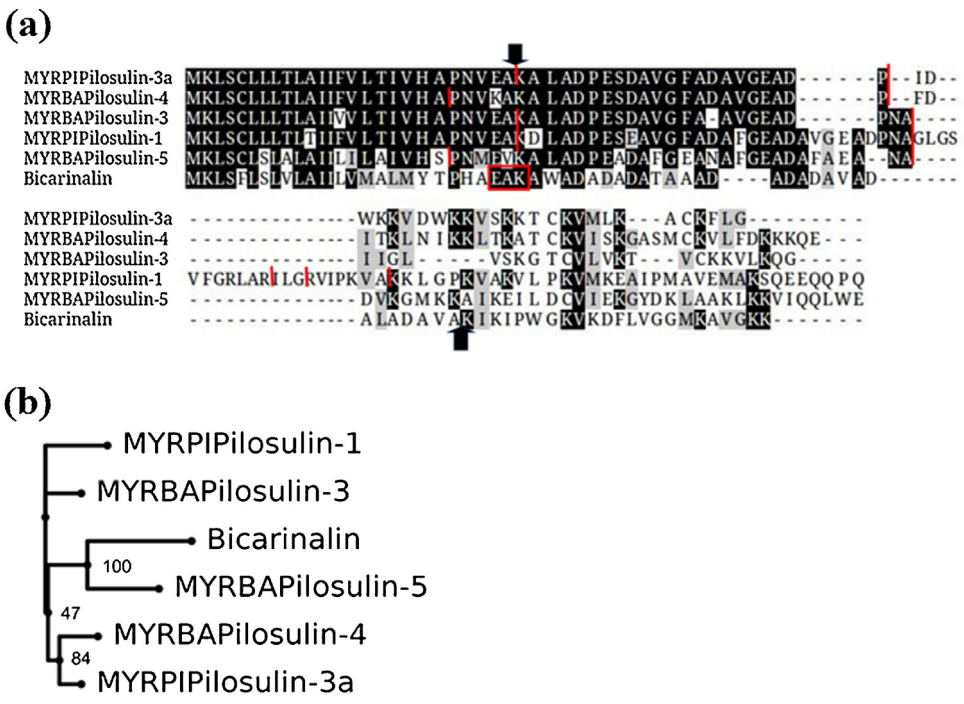

Fig. 6. **[a]** Alignment of amino acid sequences of pilosulin and bicarinalin using CLUSTAL W program. Conserved sequences are highlighted in black. Partial conservation [amino acid with the same properties] are highlighted in grey. Black arrowheads indicate the predicted processing sites for bicarilin propeptide based on signal peptide sequence prediction, sequence similarity with other pilosulin and sequence of mature peptide determined previously. Red line indicates cleavage site predicted for the different pilosulins. [MYRPI: *Myrmecia pilosula*, MYRBA: *Myrmecia banksi*], accession number uniprot: pilosulin-5: A9CM07, pilosulin-4: Q68Y22, pilosulin-3: Q68Y23, pilosulin-3a: Q26464, pilosulin-1: Q07932. The alignment of the N-terminal domain was refined manually. **[b]** Phyllogenetic tree of pilosulin and bicarinalin peptide in ants. The tree was constructed with Quicktree 1.1 program using Neighbor-Joining method. Data were re-sampled by 1000 boostrap replicates. The tree was edited with phylowidget program. (For interpretation of the references to colour in this figure legend, the reader is referred to the web version of this article.)

Lys[18] residues. These data was in good agreement with the different number of characteristic NOE cross-peaks present in the NOESY spectra (Fig. 7b). Indeed, the observation of strong to medium N,N (i,i + 1), α,N (i,i + 2) and α,N (i,i + 3) correlations between residues Trp[6] and Met[17] residues reinforced the hypothesis of a helical conformation in this region of the molecule (Fig. 7b). The presence of α,β (i,i + 3) and α,N (i,i + 4) correlations suggested that this helix is an α-helix type [31].

3.8. 3D structure of bicarinalin

A total of 156 distance restraints (64 intraresidue, 47 sequential, 19 medium range and 26 ambiguous) were deduced from NOE cross-peaks observed in the 150 ms NOESY spectrum and used for the calculations. Among the 100 generated structures, 64 structures were consistent with the experimental data and the standard covalent geometry. The structures showed no distance violations larger than 0.2 Å and no ideal geometry violations. Analysis of the Φ and Ψ angles revealed a good convergence for residues Trp[6]-Gly[16] (except for Gly[7] and ψ of Gly[16] moieties; Supplementary Table 3). These residues were located in the right-handed helix region of the Ramachandran plot (data not shown) where all bicarinalin structures exhibited a similar helical backbone folding as shown by the superimposition of the 64 final structures (Fig. 8a), <rmsd> = 0.68 Å). The Φ/Ψ values obtained for Trp[6]-Gly[16] residues were characteristic of α-helix type values. Consistent with these observations, mainly $HN_{i+4\rightarrow}CO_i$ hydrogen bonds, typical of α-helix, were observed in the structures (Supplementary Table 4). Altogether, these data indicated the presence in bicarinalin of an α – helical structure (Trp[6]-Gly[16]) flanked by two N- and C-terminal disordered regions (Fig. 8b). This helix exhibits amphipathic characteristics: hydrophilic Lys[8], Lys[10] and Asp[11] residues were located on one side of the helix, whereas the hydrophobic Val[9], Phe[12] and Leu[13] residues were on the opposite side (Fig. 8c).

4. Discussion

In the present study, we established a broad spectrum of antimicrobial activity of bicarinalin, assessed its cytotoxicity and stability in human serum, determined its secondary structure and its prepropeptide sequence.

The antimicrobial and antiparasitic activities of bicarinalin were examined in comparison to those of standard antibiotics and antifungal agents. Bicarinalin exhibited a broad-spectrum of potent anti-infective actions against Gram-positive and Gram-negative bacteria, fungi and one parasite (Leishmania) with a low cytotoxicity. Indeed, like a lot of AMPs, bicarinalin is active against numerous standard and multi-resistant strains. MICs against Gram-negative bacteria are lower than control agents (melittin or other antibiotics) even against the multi-resistant strain of *P. aeruginosa*. It was almost the same against Gram-positive bacteria except for MRSA for which melittin and tetracycline are slightly more potent. Regarding fungi and yeasts, MICs were disparate for bicarinalin as well as for fluconazole. However, *A. niger* and MDR *C. albicans* were particularly susceptible to bicarinalin compared to fluconazole suggesting an interesting opportunity in the fight against infections caused by these pathogenic organisms.

SYTOX green indicated a membrane permeabilization for all the exposed microorganisms, showing that this peptide acted by a non-specific mechanism of action. These results are consistent with our previous data on the membranolytic effect of bicarinalin on different strains of Enterobacteriaceae [22]. We can hypothesize that bicarinalin interacts with the negatively charged phospholipids to cause disruption of the cell membrane as described for a lot of cationic and cystein-free antimicrobial peptides [32].

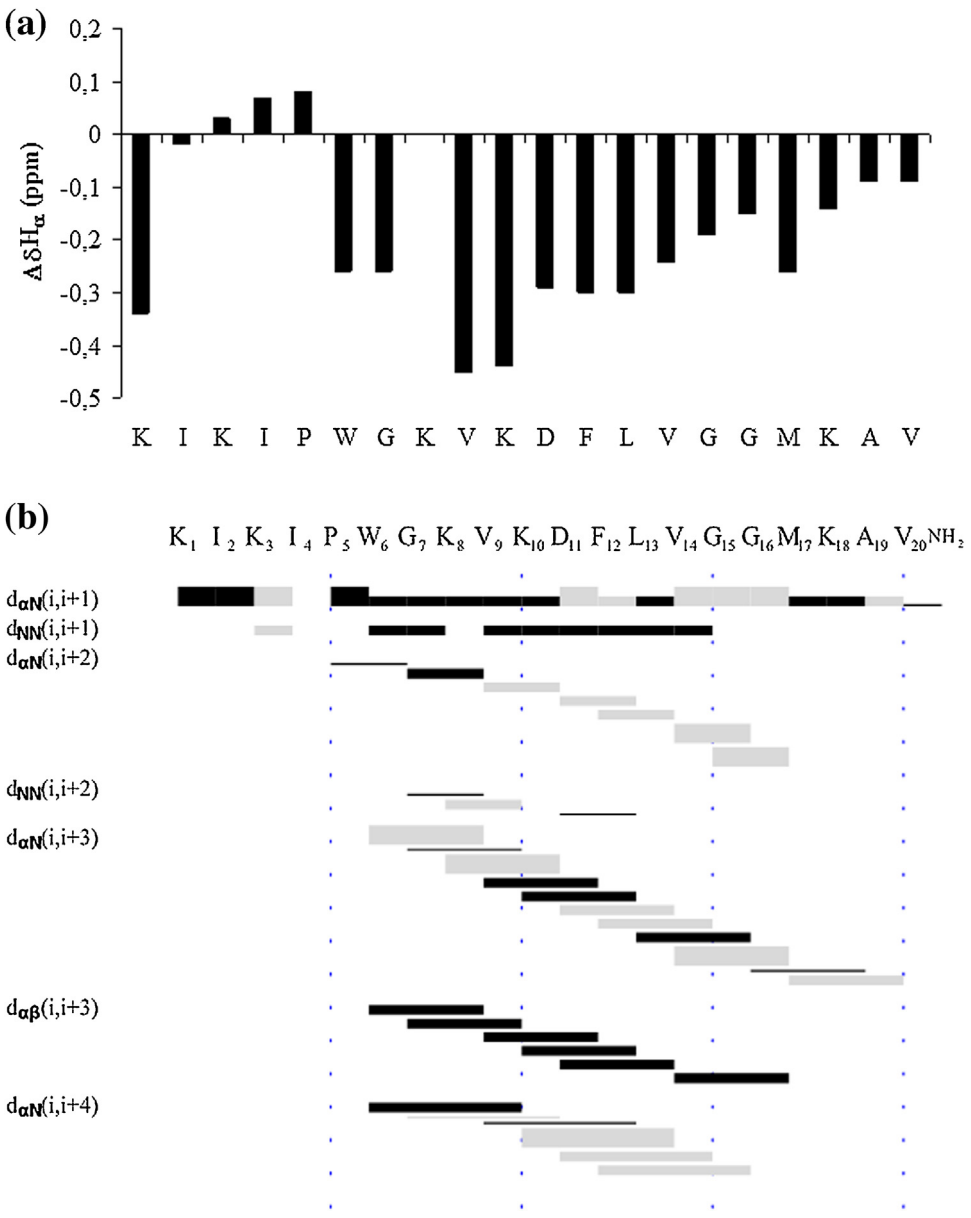

Fig. 7. [a] ^{1}Hα secondary shift in aqueous solution vs. bicarinalin peptide sequence. ^{1}Hα secondary shifts were calculated using ^{1}Hα random coil values from Wishart et al. [1995] [31]. For residue 4, the random coil values were corrected for the presence of a proline at residue $i+1$ [31]. **[b]** Summary of the sequential and medium range NOEs used for secondary structure determination of bicarinalin. The NOEs are classified into three categories [strong, medium and weak] based on the cross-peak volumes. The intensity is indicated by the thickness of the bars. Ambiguous NOEs are represented by grey lines.

Numerous mechanisms have been proposed, including the barrel-stave pore, toroidal pore, aggregate, carpet-like and detergent-like models [10]. All these models imply a first step corresponding to the interaction with the phospholipids of the membrane. Combined to the relative cytotoxicity of this peptide against human erythrocytes and lymphocytes, these data demonstrate a favorable selectivity of bicarinalin for microorganisms over mammalian cells. This selectivity is probably due to the fact that cationic peptides have a peculiar affinity for the anionic membranes of bacteria rather than for the neutral membranes of eukaryotic cells [3].

Molecular modeling under NMR restraints of bicarinalin showed a secondary structure containing a central α-helix (W^{6}-G^{16}) flanked by two flexible regions. This helix exhibited partial amphipathicity, mostly confined to the first main part of the helix (Fig. 8c). These results support the hypothesis of a mechanism of action by a membrane destabilization process. Concurrently, scrambled bicarinalin, which did not exhibit a similar α-helix, was totally devoid of antimicrobial activity (data not showed), confirming the link between the secondary structure of bicarinalin and its activity. However, since bicarinalin$_{(4–20)}$ had a MIC 2–3 folds higher than that of the parent peptide (Supplementary Table 2), we can assume that the cationic and disordered N-terminal region was also essential to the full activity of bicarinalin.

Regarding cytotoxicity, we have previously shown that bicarinalin, with an HC_{10} of 325 μmol L^{-1} is 400-fold less hemolytic than melittin, the main AMP from the honeybee venom [21]. This value is higher than the fifteen MICs determined in this study (half are lower than or equal to 6 μmol L^{-1}), suggesting a broad therapeutic window for bicarinalin or analogs. Albeit bicarinalin exhibited no toxicity against human lymphocytes for antimicrobial concentrations ranging from 0.1 to 8.5 μmol L^{-1}, it became cytotoxic for upper concentrations (LC_{50} = 67.8 μmol L^{-1}). This result shows that the hemolytic property should not be the only criterion to evaluate the therapeutic window of an antimicrobial compound. Even if this

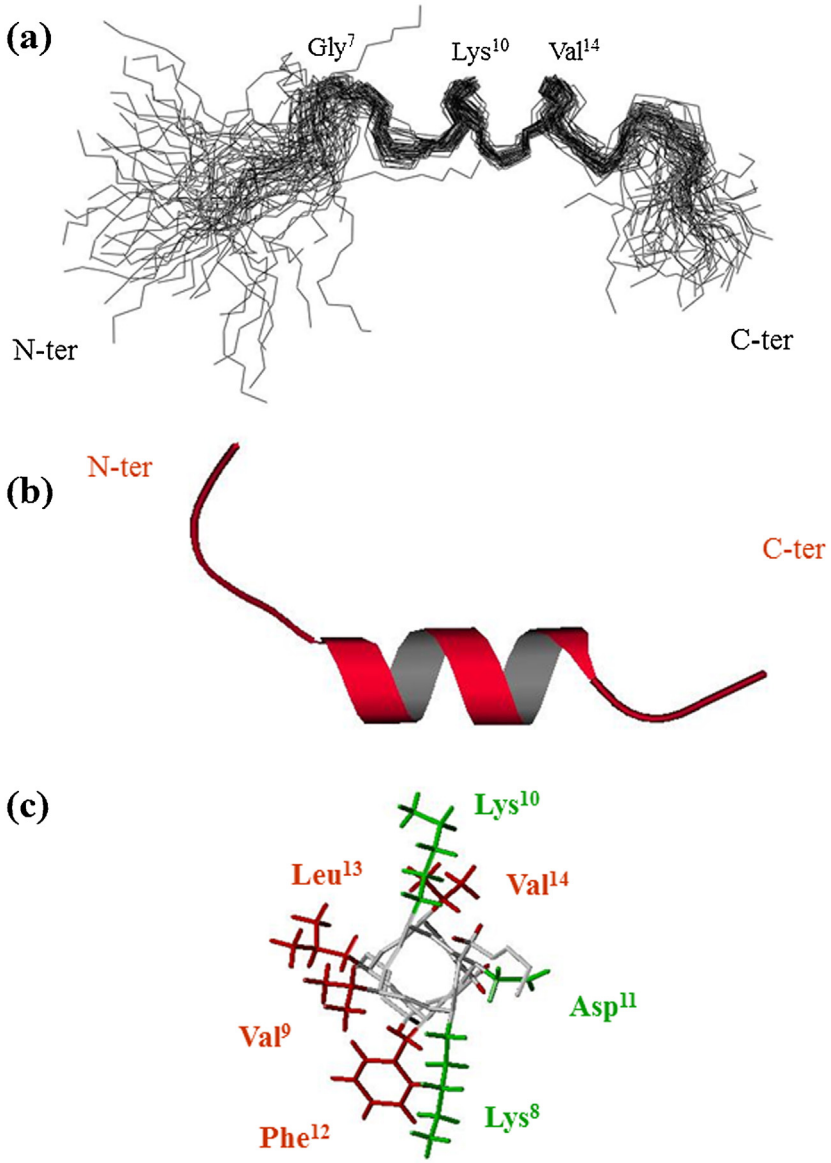

Fig. 8. **[a]** Superimposition of the 64 final structures for bicarinalin in a water/TFE mixture, aligned to obtain the best overlap of residues Trp^{6}-Gly^{16}. **[b]** Schematic representation of the bicarinalin structure in a water/TFE mixture. **[c]** Wheel projection of the bicarinalin helix residues. For clarity, Lys^{1}-Pro^{5} and Met^{17}-Val^{20} residues, as well as Trp^{6} side-chain are not represented.

cytotoxicity is nearly 10 times upper the MICs measured, it reduces its potential applications.

For preclinical development, the stability of peptides in biological fluids is generally investigated even if hepatic and renal clearances represent their main elimination processes [33]. Half-life of peptides in serum is often limited (few min [34]) thereby hampering their use as medicines [4,35]. Therefore, we used human serum as *in vitro* predictive system to characterize the putative metabolism caused by blood peptidases [34,36]. We showed that bicarinalin was still active against *S. aureus* for about 15 h after incubation in human serum. Its persistence was confirmed by LC–MS analysis. Subsequently, its activity gradually declined to disappear after 24 h of incubation. Time-course occurrence of metabolites indicated a slow degradation of bicarinalin by cleavages after the N-terminal lysines which could result from a trypsin-like proteolysis. With a relatively long half-life of bicarinalin in human serum around 15 h, these findings show a good resistance of this AMP to proteolytic action of blood peptidases.

Bicarinalin exhibited a MIC value against *S. aureus* in the same range as 30 different AMPs recently reported [37]. In particular, its MIC was very close to that of the four most active natural peptides, ascaphin-8, lycotoxin-I, maculatin-1.3 and piscidin-1 as shown in Table 2. However, it is interesting to note that most of these AMPs are hemolytic for concentrations below those observed for bicarinalin. A low MIC is not the only criterion to characterize the pharmacological potential of an AMP. For instance, melittin is a potent AMP against *S. aureus* but a poor potential drug since its therapeutic index (TI), *i.e.* the ratio between the hemolytic concentration (HC_{50}) and the MIC values [38,39], is very low (TI = 0.17; Table 2). Larger the TI, safer the drug. Thus, Table 2 shows that bicarinalin, like eumenitin, presented the highest TI (108 and 166 respectively). As previously described [41,44,45], we have calculated the relative selectivity index (RSI) of bicarinalin. Table 3 shows that the RSI of bicarinalin was higher than that of melittin, demonstrating once again the potential therapeutic interest of this peptide. However, bicarinalin was cytotoxic for lymphocytes at doses upper to 70 μmol L^{-1}. This could be an opportunity to explore

Table 2
Comparison of the therapeutic indices [TI] against *S. aureus* of bicarinalin and 9 AMPs.

Peptide name	Peptide sequence	Net charge	$MIC_{S.aureus}$ [μmol L^{-1}]	HC_{50}[a] [μmol L^{-1}]	TI[b]	ref
Bicarinalin	KIKIPWGKVKDFLVGGMKAV-NH_2	+ 6	3	325	108	
Melittin	GIGAVLKVLTTGLPALISWIKRKRQQ-NH_2	+ 5	3.5	0.6	0.17	
Eumenitin	LNLKGIFKKVASLLT	+ 3	6	>1000	>166	[40]
Coprisin	VTCDVLSFEAKGIAVNHSACALHCIALRK- −KGGSCQNGVCVCRN	+ 3	2	>100	>50	[41]
Defensin-NV	VTCELLMFGGVVGDSACAANCLSMGK-−AGGSCNGGLCDCRKTTFKELWDKRFG	+ 1	0.9	>37 [5%]	>40	[42]
Pilosulin P1	GLGSVFGRLARILGRVIPKV	+ 5	4	60	15	[43]
Lycotoxin-I	IWLTALKFLGKHAAKHLAKQQLSKL	+ 7	3.1	125	40	[37]
Ascaphin-8	GFKDLLKGAAKALVKTVLF-NH_2	+ 4	3.1	45	15	[37]
Maculatin-1.3	GLLGLLGSVVSHVVPAIVGHF-NH_2	+ 3	6.2	25	4	[37]
Piscidin-1	FFHHIFRGIVHVGKTIHRLVTG	+ 7	3.1	20	7	[37]

[a] HC_{50}: minimal peptide concentration that produces 50% of hemolysis.
[b] TI: therapeutical index [HC/MIC].

Table 3
Peptide relative selectivity index [RSI] and antimicrobial activities against standard and antibiotic-resistant bacterial strains.

Peptides	MIC [μmol L^{-1}]										GM[a]	HC_{50}[b]	RSI[c]
	Gram-negative bacteria					Gram-positive bacteria							
	E. coli	*C. sakazakii*	*P. aeruginosa*	*P. aeruginosa* [R]	*S. enterica*	*E. hirae*	*S. aureus*	*MRSA*	*S. xylosus*	*B. substilis*			
Bicarinalin	24.4	5.80	12.2	8.7	5.4	12.2	3.0	8.7	0.45	24.4	10.5	325	31
Melittin	22.4	17.2	73.9	74.5	52.7	> 97.5	3.5	3.4	2.6	89.6	43.9	0.6	0.014

[a] GM: Geometric mean of the minimum inhibitory concentration [MIC] values from all fifteen strains.
[b] HC_{50}: Minimal peptide concentration that produces 50% of hemolysis.
[c] RSI: Relative selectivity index given by the ratio of the HC [μmol L^{-1}] to the GM of the MIC [μmol L^{-1}]. Larger values indicate greater cell selectivity.

a possible anticancer potential of bicarinalin. Pharmacomodulation study, according to the strategy developed by Conlon et al. [11], could be undertaken to focus the activity of bicarinalin or analogs either as antimicrobial, or as antilymphomas agents. Collectively, these results show that bicarinalin exhibited a broad-spectrum of potent anti-infective actions with a relative low cytotoxicity.

Molecular cloning of the cDNA encoding bicarinalin precursor revealed that the N-terminal domain of bicarinalin precursor was closely related to those of pilosulins cloned in Jack jumper ant species with a higher similarity with pre-propilosulin-5 (Fig. 6). Although the genera *Tetramorium* and *Myrmicia* are phylogenetically distant, we can conclude that bicarinalin and pilosulins belongs to the same precursor family. Nevertheless, the C-terminal domain corresponding to the mature peptides has highly diverged in the course of evolution. Bicarinalin and pilosulin precursors exhibit a similar organisation with a predicted 26-amino acid signal peptide and a 22–30 N-terminal flanking propeptide, mature sequence being located at the C-terminal extremity of the precursor. They also share a canonical GXY (GKK for bicarinalin) motif at the C-terminal side thus generating a clearly established 20-residue amidated mature form of bicarinalin and suggested (Genbank) for pilosulin 3a and 3. These homologies indicate conserved processing pathways in ants. However, dibasic motif that constitutes potential cleavage sites in neuropeptide precursors or in amphibian antimicrobial prepropeptides have been poorly conserved [46,47]. In bicarinalin precursor, this cleavage site did not exist and processing is thought to occur between the AK motif of the N-terminal side of the active peptide.

In conclusion, we have established that bicarinalin showed a broad spectrum of antimicrobial activities, a good stability to blood proteases, no hemolytic activity and weak cytotoxic effects on human lymphocytes. All of these data are consistent with a good TI. Thus, bicarinalin seems to be a credible candidate for the development of a brand new antimicrobial drug. To consolidate its relevance as therapeutic agent template, the general pattern of its cytotoxicity towards different type of eukaryotic cells has to be established. More widely, bicarinalin illustrates the interest of the venom of ants as tank of new bioactive molecules.

Funding

A.R. was the recipient of a PhD fellowship from the Région Midi-Pyrénées and the University Champollion. The Urban Community of Albi and INSERM (U982), CNRS and Labex Synorg [UMR 6014] provided the financial support for research works. This work has benefited from an "Investissement d'Avenir" grant managed by the Agence Nationale de la Recherche (CEBA, ref. ANR- 10-LABX-0025).

Acknowledgments

The authors thank Sandra Roger for her technical assistance and the "Etablissement Français du Sang" (France) to have kindly provided the fresh human serum. We also thank the Centre de Ressources Informatiques de Haute-Normandie for molecular modeling facilities.

Appendix A. Supplementary data

Supplementary data associated with this article can be found, in the online version, at http://dx.doi.org/10.1016/j.peptides.2016.04.001.

References

[1] G.G. Perron, M. Zasloff, G. Bell, Experimental evolution of resistance to an antimicrobial peptide, Proc. Biol. Sci. 273 (2006) 251–256.
[2] G. Laverty, S.P. Gorman, B.F. Gilmore, The potential of antimicrobial peptides as biocides, Int. J. Mol. Sci. 12 (2011) 6566–6596.
[3] M. Zasloff, Antimicrobial peptides of multicellular organisms, Nature 415 (2002) 389–395.
[4] N. Brogden, K. Brogden, Will new generations of modified antimicrobial peptides improve their potential as pharmaceuticals, Int. J. Antimicrob. Agents 38 (2012) 217–225.
[5] N.Y. Yount, M.R. Yeaman, Emerging themes and therapeutic prospects for anti-infective peptides, Annu. Rev. Pharmacol. Toxicol. 52 (2012) 337–360.
[6] A. Giuliani, G. Pirri, S.F. Nicoletto, Antimicrobial peptides: an overview of a promising class of therapeutics, Cent. Eur. J. Biol. 2 (2007) 1–33.
[7] S.E. Löfgren, L.C. Miletti, M. Steindel, E. Bachère, M. Barracco, Trypanocidal and leishmanicidal activities of different antimicrobial peptides [AMPs] isolated from aquatic animals, Exp. Parasitol. 118 (2008) 197–202.
[8] J. Slaninová, V. Mlsová, H. Kroupová, L. Alán, T. Tůmová, L. Monincová, L. Borovičková, V. Fučík, V. Ceřovský, Toxicity study of antimicrobial peptides

from wild bee venom and their analogs toward mammalian normal and cancer cells, Peptides 33 (2012) 18–26.
[9] W.C. Wimley, K. Hristova, Antimicrobial peptides: successes, challenges and unanswered questions, J Membrane Biol 239 (2011) 27–34, http://dx.doi.org/10.1007/s00232-011-9343-0.
[10] L.T. Nguyen, E.F. Haney, H.J. Vogel, The expanding scope of antimicrobial peptide structures and their modes of action, Trends Biotechnol. 29 (9) (2011) 464–472.
[11] J.M. Conlon, N. Al-Ghaferi, B. Abraham, J. Leprince, Strategies for transformation ofnaturally-occurring amphibian antimicrobial peptides into therapeutically valuable anti-infective agents, Methods 42 (2007) 349–357.
[12] L. Cao, C. Dai, Z. Li, Z. Fan, Y. Song, Y. Wu, Z. Cao, W. Li, Antibacterial activity and mechanism of a scorpion venom peptide derivative *in vitro* and *in vivo*, PLoS One 7 (2012) e40135.
[13] V. Cerovský, J. Slaninová, V. Fucík, H. Hulacová, L. Borovicková, R. Jezek, L. Bednárová, New potent antimicrobial peptides from the venom of Polistinae wasps and their analogs, Peptides 29 (2008) 992–1003.
[14] L. Kuhn-Nentwig, Antimicrobial and cytolytic peptides of venomous arthropods, Cell. Mol. Life Sci. 60 (2003) 2651–2668.
[15] R. Stöcklin, P. Favreau, R. Thai, J. Pflugfelder, P. Bulet, D. Mebs, Structural identification by mass spectrometry of a novel antimicrobial peptide from the venom of the solitary bee Osmia rufa [Hymenoptera: megachilidae], Toxicon 55 (2010) 20–27.
[16] AntCat 2015 Retrieved from: http://www.antcat.org/ (05.01.16).
[17] N.W. Davies, M.D. Wiese, S.G. Brown, Characterisation of major peptides in Jack jumper ant venom by mass spectrometry, Toxicon 43 (2004) 173–183.
[18] H. Inagaki, M. Akagi, H.T. Imai, R.W. Taylor, M.D. Wiese, N.W. Davies, T. Kubo, Pilosulin 5 a novel histamine-releasing peptide of the Australian ant, *Myrmecia pilosula* [Jack Jumper Ant], Arch. Biochem. Biophys. 477 (2008) 411–416.
[19] J. Orivel, V. Redeker, J.P. Le Caer, F. Krier, M. Revol-Junelles, A. Longeon, A. Chaffotte, A. Dejean, J. Rossier, Ponericins, new antibacterial and insecticidal peptides from the venom of the ant *Pachycondyla goeldii*, J. Biol. Chem. 276 (2001) 17823–17829.
[20] S.R. Aili, A. Touchard, P. Escoubas, M.P. Padula, J. Orivel, A. Dejean, G.M. Nicholson, Diversity of peptide toxins from stinging ant venoms, Toxicon 92 (2014) 166–178.
[21] A. Rifflet, S. Gavalda, N. Téné, J. Orivel, J. Leprince, L. Guilhaudis, E. Génin, A. Vétillard, M. Treilhou, Identification and characterization of a novel antimicrobial peptide from the venom of the ant *Tetramorium bicarinatum*, Peptides 38 (2012) 363–370.
[22] N. Téné, V. Roche-Chatain, A. Rifflet, E. Bonnafé, B. Lefranc, J. Leprince, M. Treilhou, Potent bactericidal effects of bicarinalin against strains of the Enterobacter and Cronobacter genera, Food Control 42 (2014) 202–206.
[23] D. Sereno, P. Holzmuller, I. Mangot, G. Cuny, A. Ouaissi, J.-L. Lemestre, Antimonial-mediated DNA fragmentation in *Leishmania infantum* amastigotes, Antimicrob. Agents Chemother 45 (2001) 2064–2069.
[24] A. Brünger, P. Adams, G. Clore, W. DeLano, P. Gros, R. Gross-Kinstleve, J. Jiang, J. Kuszewski, M. Nilges, N. Pannu, R. Read, L. Rice, T. Simonson, G. Warren, Crystallography & NMR System: a new software suite for macromolecular structure determination, Acta Crystallogr. Sect. D Biol. Crystallogr. 54 (1998) 905–921.
[25] E. Stein, L. Rice, A. Brünger, Torsion-angle molecular dynamics as a new efficient tool for NMR structure calculation, J. Magn. Reson. (1997) 154–164.
[26] P. Kraulis, MOLSCRIPT: a program to produce both detailed and schematic plots of protein structures, J. Appl. Crystallogr. (1991) 946–950.
[27] S. Nemati, R. Hassanzadeh, S. Khajeh Jahromi, A. Delkhosh Nasrollah Abadi, Otomycosis in the north of Iran: common pathogens and resistance to antifungal agents, Eur. Arch. Otorhinolaryngol 271 (2014) 953–957.
[28] M. Zanetti, R. Gennaro, D. Romeo, Cathelicidins: a novel protein family with a common proregion and a variable C-terminal antimicrobial domain, FEBS Lett. 374 (1995) 1–5.
[29] D.J. Merkler, C-terminal amidated peptides: production by the *in vitro* enzymatic amidation of glycine-extended peptides and the importance of the amide to bioactivity, Enzyme Microb. Technol. 16 (1994) 450–456.
[30] K. Wüthrich, M. Billeter, W. Braun, Polypeptide secondary structure determination by nuclear magnetic resonance observation of short Proton-proton distances, J. Mol. Biol. 180 (1984) 715–740.
[31] D.S. Wishart, C.G. Bigam, A. Holm, R.S. Hodges, B.D. Sykes, 1[H], [13]C and [15]N random coil NMR chemical shifts of the common amino acids. Part I. Investigations of nearest-neighbor effects, J. Biomol. NMR 5 (2016) 67–81.
[32] P.F. Almeida, A. Pokorny, Mechanisms of antimicrobial, cytolytic, and cell-penetrating peptides: from kinetics to thermodynamics, Biochemistry 48 (2009) 8083–8093.
[33] H. John, K.D. Huynh, C. Hedtmann, M. Walden, A. Schulz, F.B. Anspach, W.-G. Forssmann, In vitro degradation of the antimicrobial human peptide HEM-gamma 130–146 in plasma analyzed by a validated quantitative LC–mS/MS procedure, Anal. Biochem 341 (2005) 173–186.
[34] C. Neveu, B. Lefranc, O. Tasseau, J.-C. Do-Rego, A. Bourmaud, P. Chan, P. Bauchat, O. Le Marec, J. Chuquet, L. Guilhaudis, Boutin J. a, I. Ségalas-Milazzo, J. Costentin, H. Vaudry, M. Baudy-Floc'h, D. Vaudry, J. Leprince, Rational design of a low molecular weight, stable, potent, and long-lasting GPR103 aza-β3-pseudopeptide agonist, J. Med. Chem. 55 (2012) 7516–7524.
[35] H. John, Liquid chromatography-mass spectrometry in peptide drug discovery and development, Anal. Bioanal. Chem 381 (2005) 51–53.
[36] K. Sanderson, P.E. Andrén, R.M. Caprioli, F. Nyberg, In vitro metabolism of LVV-hemorphin-7 in human plasma studied by reversed-phase high-performance liquid chromatography and micro-electrospray mass spectrometry, J. Chromatogr. A 743 (1996) 207–212.
[37] J. Menousek, B. Mishra, M.L. Hanke, C.E. Heim, T. Kielian, G. Wang, Database screening and *in vivo* efficacy of antimicrobial peptides against methicillin-resistant *Staphylococcus aureus* USA300, Int. J. Antimicrob. Agents 39 (2012) 402–406.
[38] M. Fázio, L. Jouvensal, F. Vovelle, P. Bulet, M.T. Miranda, S. Daffre, A. Miranda, Biological and structural characterization of new linear gomesin analogues with improved therapeutic indices, Biopolymers 88 (2007) 386–400.
[39] Y. Chen, C.T. Mant, S.W. Farmer, R.E. Hancock, M.L. Vasil, R.S. Hodges, Rational design of α-helical antimicrobial peptides with enhanced activities and specificity/Therapeutic Index, J. Biol. Chem. 280 (2005) 12316–12329.
[40] K. Konno, M. Hisada, H. Naoki, Y. Itagaki, R. Fontana, M. Rangel, J.S. Oliveira, M.P. Cabrera, J.R. Neto, I. Hide, Y. Nakata, T. Yasuhara, T. Nakajima, Eumenitin, a novel antimicrobial peptide from the venom of the solitary eumenine wasp *Eumenes rubronotatus*, Peptides 27 (2006) 2624–2631.
[41] E. Lee, J.K. Kim, S. Shin, K.W. Jeong, A. Shin, J. Lee, D.G. Lee, J.S. Hwang, Y. Kim, Insight into the antimicrobial activities of coprisin isolated from the dung beetle, *Copris tripartitus*, revealed by structure-activity relationships, Biochim. Biophys. Acta 1828 (2013) 271–283.
[42] J. Ye, H. Zhao, H. Wang, J. Bian, R. Zheng, A defensin antimicrobial peptide from the venoms of *Nasonia vitripennis*, Toxicon 56 (2010) 101–106.
[43] I. Zelezetsky, U. Pag, N. Antcheva, H.-G. Sahl, A. Tossi, Identification and optimization of an antimicrobial peptide from the ant venom toxin pilosulin, Arch. Biochem. Biophys. 434 (2005) 358–364.
[44] P. Wang, Y.H. Nan, S.-T. Yang, S.W. Kang, Y. Kim, I.-S. Park, K.-S. Hahm, S.Y. Shin, Cell selectivity and anti-inflammatory activity of a Leu/Lys-rich alpha-helical model antimicrobial peptide and its diastereomeric peptides, Peptides 31 (2010) 1251–1261.
[45] E.K. Lee, Y.-C. Kim, Y.H. Nan, S.Y. Shin, Cell selectivity, mechanism of action and LPS-neutralizing activity of bovine myeloid antimicrobial peptide-18 [BMAP-18] and its analogs, Peptides 32 (2011) 1123–1130.
[46] N. Chartrel, C. Dujardin, Y. Anouar, J. Leprince, A. Decker, S. Clerens, J.-C. Do-Rego, F. Vandesande, C. Llorens-cortes, J. Costentin, J. Beauvillain, H. Vaudry, Identification of 26RFa, a hypothalamic neuropeptide of the RFamide peptide family with orexigenic activity, Proc.Natl. Acad. Sci. U. S. A. 100 (2003) 15247–15252.
[47] E. Iwakoshi-Ukena, M. Soga, G. Okada, T. Fujii, M. Sumida, K. Ukena, Characterization of novel antimicrobial peptides from the skin of the endangered frog *Odorrana ishikawae* by shotgun cDNA cloning, Biochem. Biophys. Res. Commun. 412 (2011) 673–677.